

Formation of Helical Protein Assemblies of IgG and Transducin on Varied Lipid Tubules

Thomas J. Melia, Mathew E. Sowa,* Linda Schutze, and Theodore G. Wensel*,¹

Verna and Marrs McLean Department of Biochemistry and *Structural and Computational Biology and Molecular Biophysics Program, Baylor College of Medicine, Houston, Texas 77030

Received April 1, 1999, and in revised form June 7, 1999

Helical protein arrays on lipid tubules are valuable assemblies for studying protein structure and protein–lipid interactions through electron microscopy and crystallography. We describe conditions for forming such arrays from two proteins, IgG and transducin, the photoreceptor G protein, using a variety of lipid surfaces. Anti-dinitrophenyl (DNP) IgG arrays formed on DNP–phosphatidylethanolamine (DNP–PE) mixed with either galactosylceramide lipids or phosphatidylcholine (PC) display different pH sensitivities and dimensions, yet have similar helical symmetries. DNP–PE/PC mixtures formed small crystals and large well-ordered flattened tubules. The peripheral membrane protein transducin (G_t) formed helical arrays either on a mixture of cationic and neutral lipids or on residual photoreceptor lipids. Despite differences in lipid composition, the G_t arrays have similar structures and show similar sensitivity to activation and variations in ionic environment. G_t activation causes the helical assemblies to collapse to small vesicles, a process resembling the vesiculation of activated dynamin–lipid tubules. In a preliminary three-dimensional reconstruction, the haptin-bound IgG appears to make two contacts to the central lipid tubule, presumably via the F_{ab} domains. The ability to generate a three-dimensional reconstruction without tilts illustrates one advantage of helical structures for two-dimensional crystallography, especially for visualizing protein–lipid interactions.

© 1999 Academic Press

INTRODUCTION

Electron crystallography is a powerful method for studying the structure and function of proteins that form large complexes, that are membrane associ-

ated, or for which the amounts of sample are limited. The vast majority of moderate-sized soluble proteins studied by EM have been solved from two-dimensional crystals grown on lipid monolayers (Uzgiris and Kornberg, 1983). The lipid layer approach depends upon tight protein–lipid interactions and is often facilitated by the introduction of modified lipids with covalently attached protein-binding sites. Analysis of these crystals is often hampered by the difficulty of transferring a stable intact lipid monolayer to the electron microscope grid and by the need to collect a tilt series in the microscope in order to retrieve three-dimensional information. Recently, several groups have identified sample conditions allowing soluble proteins to form helical crystals on the surfaces of lipid tubules (Polyakov *et al.*, 1995; Ringler *et al.*, 1997; Sweitzer and Hinshaw, 1998; Takei *et al.*, 1998; Wilson-Kubalek *et al.*, 1998), eliminating the need for tilt series and allowing the manipulation of samples in solution or suspension rather than at the air–monolayer–water interface. To this end, Wilson-Kubalek *et al.* (1998) have identified a specific class of lipids, the galactosylceramide glycolipids, which naturally form tubules that can serve as cylindrical substrates for helical assembly. While this is an exciting emerging approach in electron crystallography, there are still relatively few examples of its application, and little is known about different proteins' influence and packing on different lipid tubules.

Parameters that guide tubule formation may also be important *in vivo* as suggested by the membrane-binding protein, dynamin, which has been shown to induce tubule formation from otherwise nontubular native membranes (Hinshaw and Schmid, 1995; Takei *et al.*, 1995). Activation of dynamin causes both the native tubular structures and those originating from liposomes to vesiculate (Hinshaw and Schmid, 1995; Sweitzer and Hinshaw, 1998; Takei *et al.*, 1995, 1998), suggesting that conditions that alter the assembly of ordered membrane-associated pro-

¹ To whom correspondence should be addressed at Department of Biochemistry, Baylor College of Medicine, One Baylor Plaza, Houston, TX 77030. Fax: (713) 796-9438. E-mail: twensel@bcm.tmc.edu.

tein arrays may also modulate the structure of the membrane surfaces.

To better understand protein–lipid interactions in the formation of helical protein assemblies on lipid tubules, we have explored the parameters of their formation using two different proteins: IgGs bound to hapten-derivatized lipids, one of the best characterized interactions for formation of planar 2-D crystals (Uzgiris and Kornberg, 1983), and the G protein transducin, a molecule whose lipid-binding properties are central to its physiological function and whose binding and hydrolysis of GTP are tied to important structural changes, as observed for dynamin.

Anti-DNP IgG was among the first proteins crystallized using the lipid layer technique (Uzgiris and Kornberg, 1983), by introduction of lipids with a covalently attached DNP moiety (DNP–PE) into the monolayer. Projection structures of two-dimensional crystals had a hexagonal lattice that suggested a trimeric packing of F_{ab} domains from individual IgG molecules (Uzgiris and Kornberg, 1983). The authors proposed that both F_{ab} s were associated with DNP–PE, positioning the IgG in a plane parallel to the membrane. Ultimately, however, determination of the packing and orientation of the IgG molecules requires a three-dimensional reconstruction. Because the protein and the lipids are readily available, and because the structures of IgG's domains and location of the combining sites are well known, IgG makes an appropriate test sample for investigating protein–tubule-forming parameters.

The heterotrimeric G protein (see review by Wensel, 1999) transducin (G_t) is found in the rod photoreceptor cells of the retina and is responsible for mediating the visual signal transduction cascade on photoreceptor disc membranes (Fung *et al.*, 1981). It is a peripherally associated membrane protein bound to the membrane through two covalently attached lipid modifications, a myristoyl group on the α subunit and a farnesyl group on the γ subunit. The X-ray structure of the heterotrimer (Lambright *et al.*, 1996) is missing these modifications but suggests that the two species may be close together in space and act as a single membrane insertion site. To determine how the protein interacts with the membrane, it will be necessary to solve its structure bound to a lipid surface. We have characterized conditions that lead to the formation of small crystalline arrays using the lipid layer technique (T.M., unpublished observations), but these have not proven suitable for structural studies. We present here conditions for forming helical tubules that present a more tractable substrate for determining the structure of the G_t –membrane complex.

METHODS

Materials and Reagents

Hypotonic Buffer A is composed of 5 mM Tris, 0.5 mM $MgCl_2$, pH 7.4, 1 mM DTT. Hypotonic Buffer B is made up of 10 mM Mops, 2 mM $MgCl_2$, pH 7.4, 1 mM DTT. Hypotonic Buffer C is composed of 10 mM Mops, 10 mM $MgCl_2$, pH 7.4, 1 mM DTT. IgG Buffer A is made of 25 mM Tris, pH 7.4, 150 mM NaCl. IgG Buffer B is composed of 10 mM PO_4 , 150 mM NaCl. G_t tubule buffer is made of 10 mM Mops, pH 7.4, 2 mM $MgCl_2$, 1 mM DTT. All buffers were filtered through 0.2- μ m nitrocellulose immediately before use. Buffers used in the purification of rod outer segment (ROS) or G_t also contained a small amount of solid protease inhibitor, phenylmethylsulfonyl fluoride (PMSF, Boehringer Mannheim). All lipids were purchased from Avanti in $CHCl_3$ and were stored at $-80^\circ C$, unless otherwise noted. Rat anti-DNP IgG $_{\kappa 1}$ monoclonal was purchased from Zymed.

G_t Purification

Purified bleached bovine ROS membranes were stripped of most peripherally associated membrane proteins by washing in moderate and hypotonic buffers (Melia *et al.*, 1997). G_t remains associated with these bleached membranes through complex formation with activated rhodopsin. Crude G_t was extracted from these washed ROS using GTP and hypotonic A buffer. GTP addition activates G_t , resulting in separation of its α and $\beta\gamma$ subunits (Fung, 1983) and release from rhodopsin. After the ROS were removed via centrifugation, the G_t -containing supernatant was collected. Because isolated G_{ta} hydrolyzes GTP in about 30 s (Navon and Fung, 1984), this supernatant contains reassociated heterotrimers. This protein, which is >85% G_t , is hereafter referred to as “crude G_t .” For some studies with activated G_{ta} -GTP γ S, the crude G_t was prepared with GTP γ S instead of GTP and contained dissociated subunits. For most experiments, G_t was further purified on one or both of the following columns. For hexylagarose purified G_t , crude G_t was collected and concentrated, exchanged into hypotonic B buffer, and loaded onto an open hexylagarose (Sigma) column. The protein was eluted in increasing [NaCl]. In some experiments, this protein was further purified by concentrating the cleanest peaks off of the hexylagarose column, changing the buffer to hypotonic C, loading onto an HPLC anion-exchange column (Waters DEAE-5PW), and eluting in increasing [NaCl]. All purified protein was stored in 40–50% glycerol at $-20^\circ C$.

Phosphate Analysis of Crude G_t

Chloroform/methanol extraction was used to isolate the residual phospholipid in crude G_t . One volume of crude G_t in hypotonic A buffer was extracted against 1 vol of 2:1 (v/v) chloroform/methanol. Control experiments with known quantities of phospholipid demonstrated quantitative recovery from the extraction. Phospholipid concentrations were determined by total phosphate analysis using a well-characterized colorimetric method (Chen *et al.*, 1956).

Aluminum Fluoride Activation of G_t

Purified G_t (0.2 mg/ml) was mixed with 1 mM NaF in G_t tubule buffer and activated with 30 μ M $AlCl_3$. In control samples, 1 mM NaCl substituted for NaF and $AlCl_3$.

Helical Crystallization of IgG

On GalCer lipid tubules. Galactosylcerebrosides (Type II Bovine Brain Lipids (Sigma C-1516)), containing galactosyl ceramide (GalCer), were stored in chloroform:isopropanol:water (70:29:1) at $-20^\circ C$ at a concentration of 5 mg/ml. DNP–PE (30% w/w) was added to GalCer, dried under a stream of argon, and

vacuum-dried overnight. Tubules were formed by resuspending the lipid mixture in IgG Buffer A to a final concentration of 1 mg/ml. Lipids were diluted 1:50 and IgG was added to a final concentration of 0.2 mg/ml. Samples were incubated for >12 h at room temperature and then 5 μ l was applied to a carbon-coated continuous nitrocellulose EM grid and stained with 1% uranyl-acetate.

From monolayers with egg-PC or DOPC. PC-containing tubules were formed using the lipid layer technique under monolayers consisting of 5–20% DNP-caproyl-phosphatidylethanolamine (DNP-PE) and 80–95% dioleoyl-phosphatidylcholine (DOPC) or egg 1- α -lecithin-phosphatidylcholine (egg-PC). Although a range of conditions resulted in helical crystals (Table I), we primarily used the following standard conditions, which lead to reproducible and efficient tubule production: 0.3 mg/ml IgG in IgG Buffer B (pH 8.4) was pipetted into clean Teflon wells. A monolayer of 5% DNP-PE, 95% egg-PC (in chloroform:hexane 1:1, 1.0 mg/ml lipid) was floated on the solution and the Teflon dish was sealed in a glass petri dish under an argon blanket for 15–18 h at room temperature before being transferred to continuous carbon-coated nitrocellulose on nickel electron microscope grids. When nitrocellulose-covered copper grids were applied to the well, the solution turned blue, suggesting that metal ions were being leached off the grid in significant quantities, likely explaining the grid-type dependence observed in Table I.

Helical Crystallization of G_t

Conditions for helical crystallization were first determined using the lipid layer technique (Uzgiris and Kornberg, 1983), in an attempt to form two-dimensional crystals. G_t (0.2 mg/ml in G_t tubule buffer) was pipetted into 12- μ l Teflon wells and \sim 1 μ l of a 0.5–1 mg/ml lipid mixture (20:80 mol/mol dioleoyl-trimethylammonium-propane (DOTAP): diphytanoyl-PC) in 1:1 v/v chloroform:hexane was layered on top to form a lipid monolayer. The Teflon plates were kept on damp filter paper in glass petri dishes at 4°C for 2 h before the sample was transferred to electron microscope grids. Although tubules were first discovered in the transfer with the monolayer, they were also found in the subphase. The presence of tubules in the subphase may either reflect the formation of helical arrays on lipid surfaces other than the monolayer (e.g., on vesicles that form as the result of excess lipid applied during the formation of the monolayer or aggregated lipid on the edges of the well) or simply indicate that the helical arrays are denser than the surrounding buffer and sink over the course of the experiment. In the case of crude G_t , tubules could be formed simply by dilution of crude G_t into G_t tubule buffer in a microcentrifuge tube. Tubules prepared in this way were collected by centrifugation and resuspension of the tubule-containing pellet.

Grid Preparation

Samples were applied to electron microscope grids (400 mesh copper grids unless otherwise noted (see Table I); Ted Pella) that were covered with a carbon-coated holey film prepared from a cellulose-acetate-butyrate (Triafol) solution (Fukami and Adachi, 1965; Toyoshima, 1989) or with a carbon-coated continuous nitrocellulose (E. F. Fullam, Inc., New York) film. The sample was transferred to the grid either by floating the grid on the monolayer for a few minutes (for the lipid layer technique) or by pipetting a 4- to 5- μ l volume directly onto the grid (for samples in microcentrifuge tubes or in the monolayer subphase). Excess sample was wicked away with filter paper and the grid was washed with 5–10 μ l buffer before either negative staining or plunging into ice. For negative stain, each grid was washed with 5–10 μ l of 1% uranyl acetate (Ted Pella). To freeze in vitreous ice, the sample was rapidly plunged into liquid ethane and maintained under liquid nitrogen until use.

Electron Microscopy and Image Digitization

Images were collected on a Jeol 100CX, a Phillips CM12, or a Zeiss 902 CEM operating at 80 kV and nominal magnifications of 30,000–50,000 \times . Images were taken on Kodak 4489 film with a 100- μ m objective aperture and were digitized on a Zeiss SCAI microdensitometer with a 7- μ m step size and twofold averaging equivalent to 4.66–2.80 \AA /pixel, depending on the magnification.

Image Processing

Straight segments of tubule images were computationally isolated and floated into a square area before the Fourier transform was calculated using the software package I.C.E. (Hardt *et al.*, 1996). Analysis and indexing of the computed Fourier transforms were carried out predominantly in SPECTRA (Schmid *et al.*, 1993a).

Helical Reconstruction

Layer line extraction and Fourier-Bessel inversion were performed with helical reconstruction programs (Schmid *et al.*, 1993b) based on the original MRC helical reconstruction algorithms (DeRosier and Moore, 1970). Reconstructions were carried out using individual images of negatively stained DNP-PE/DOPC IgG tubules. The structures were displayed and manipulated with the Explorer software package. Domains of IgG from the X-ray crystallographic structure of IgG_{2a} (Harris *et al.*, 1997) were fit visually into the density of the reconstructions.

RESULTS

IgG Tubule Formation

IgG tubules were grown on two different lipid systems, with or without GalCer. Under buffer and pH conditions similar to those that promote two-dimensional crystallization on DNP-PE monolayers (Uzgiris and Kornberg, 1983), we formed well-ordered helical assemblies on mixtures of DNP-PE and bovine brain galactosyl-ceramide (GalCer). IgG-GalCer tubules are approximately 33 nm in diameter (Fig. 1A), compared to the 30- to 50-nm-diameter of the protein-free DNP-PE/GalCer tubules alone, suggesting that IgG binding is selective for, or induced formation of, smaller diameter lipid tubules. The regular order of the IgG-GalCer tubules is visible in the electron micrograph (Fig. 1A) and more obvious in Fourier-filtered images (Fig. 1B). The computed Fourier transforms (FT) display strong layer lines out to a resolution of 3.1 nm (Fig. 1C).

In contrast, the same IgG protein exposed to monolayers containing DNP-PE and either egg-PC or DOPC displayed no tendency to order at any pH below 8.2. Above pH 8.2, we observed both small ordered planar arrays (data not shown) and large tubules (Fig. 2), suggesting that ionizable protein residues with pK_a values in the basic region may be important for array formation on these neutral surfaces. Stabilizing interactions due to the carbohydrate head group on the GalCer-containing lipids may compensate for effects of a higher net protein charge at lower pH values. In previous studies IgG arrays formed on hapten-bearing lipid layers at pH

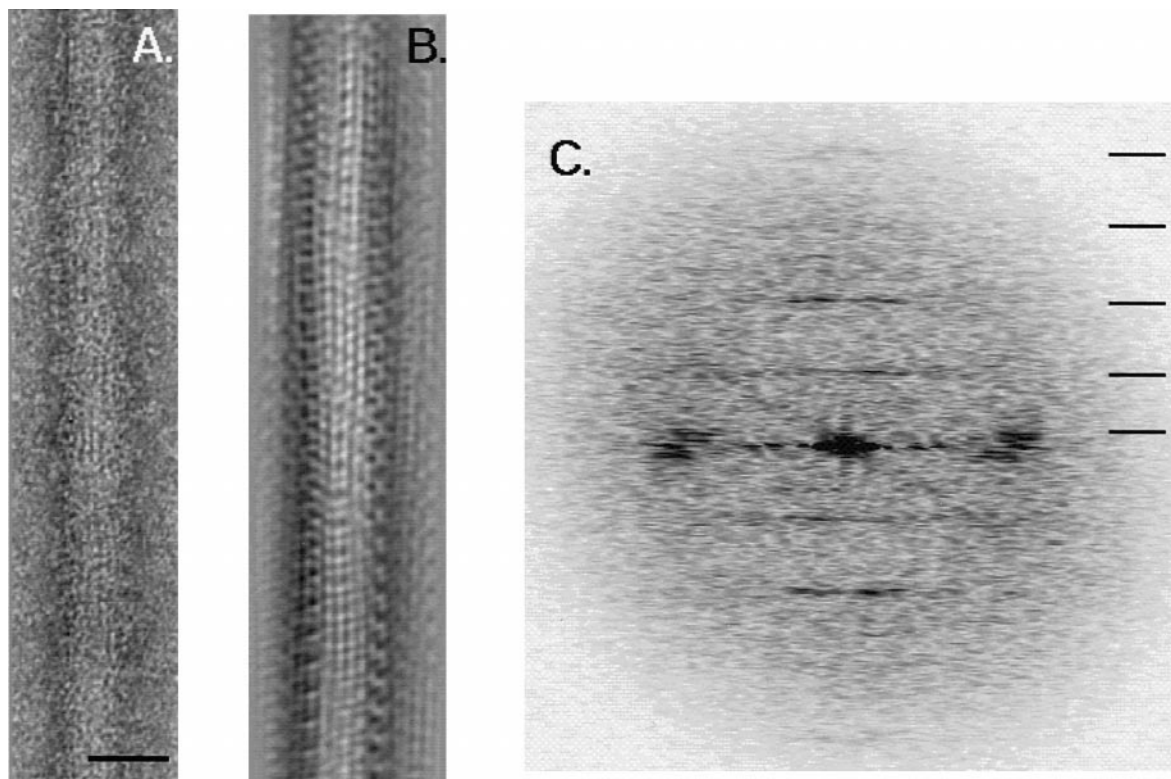


FIG. 1. Helical tubules of IgG on DNP-PE:GalCer lipids. (A) Micrograph of negatively stained tubules formed by anti-DNP IgG incubated with the tubule forming galactosyl-ceramide lipids and DNP-PE (70:30 GalCer:DNP-PE) in IgG Buffer A. The width of the tubule is approximately 28 nm (scale bar, 30 nm). (B) Filtered image, generated using the equatorial, 12.9-nm, and 6.2-nm layer lines in the computed Fourier transform (C). The lines correspond to layer lines observed at resolutions of 239, 12.9, 6.2, 4.1, and 3.1 nm.

values below 8.2; however, the amino acid sequence of the rat IgG_{K1} used here is not identical to that of the antibodies used in these previous studies, so it is not surprising that crystallization conditions differ somewhat.

The tubules were larger (~56 nm diameter) than those formed with GalCer lipids. Helical array formation required specific protein concentrations and buffer conditions (Table I), and the lipids alone did not form tubular structures. FTs from these tubules bear a striking similarity to those from the IgG-GalCer tubules (Figs. 1C and 2B), with strong layer lines detectable in both at ~12-, ~6-, and ~4-nm resolution. These similarities indicate that the protein likely packs onto these different tubules with similar lattices. In some cases, large flattened tubules, which can be treated as mosaics of two crystalline arrays, are even better ordered and contain reflections to beyond 3.0-nm resolution (Figs. 2C and 2D).

Fourier Transform Indexing

We first determined an appropriate indexing lattice for FTs computed from the crystalline flattened tubules, which could then be directly applied to FTs

from the helical nonflattened samples grown on DNP-PE:phosphatidylcholine monolayers. Comparison of phases from the near and far reflections were consistent with our Bessel order (n) determination, which was calculated by solving for $J_n = 2\pi rR$, where r is the real space radius of the tubule (~28 nm) and R is the radial position of the first maximum along the layer line. Layer line 1 is just off the equator and describes a helix with a 239-nm helical repeat. The FT is dominated by the strongest reflections at layer lines 1 and 40, with Bessel orders of 7 and 1, respectively.

We have also collected some images in vitreous ice (Fig. 2E), which show tubules of similar dimensions and helical order. There appears to be variability in the axial position of the first layer line from images in ice (Fig. 2F), perhaps reflecting a variable superhelical component.

Helical Reconstruction of an IgG-Lipid Tubule

Figure 3 shows our preliminary three-dimensional reconstruction of an IgG-lipid helical assembly determined from a single negatively stained tubule, which is representative of most of our images. While this reconstruction suffers from noise and low resolution

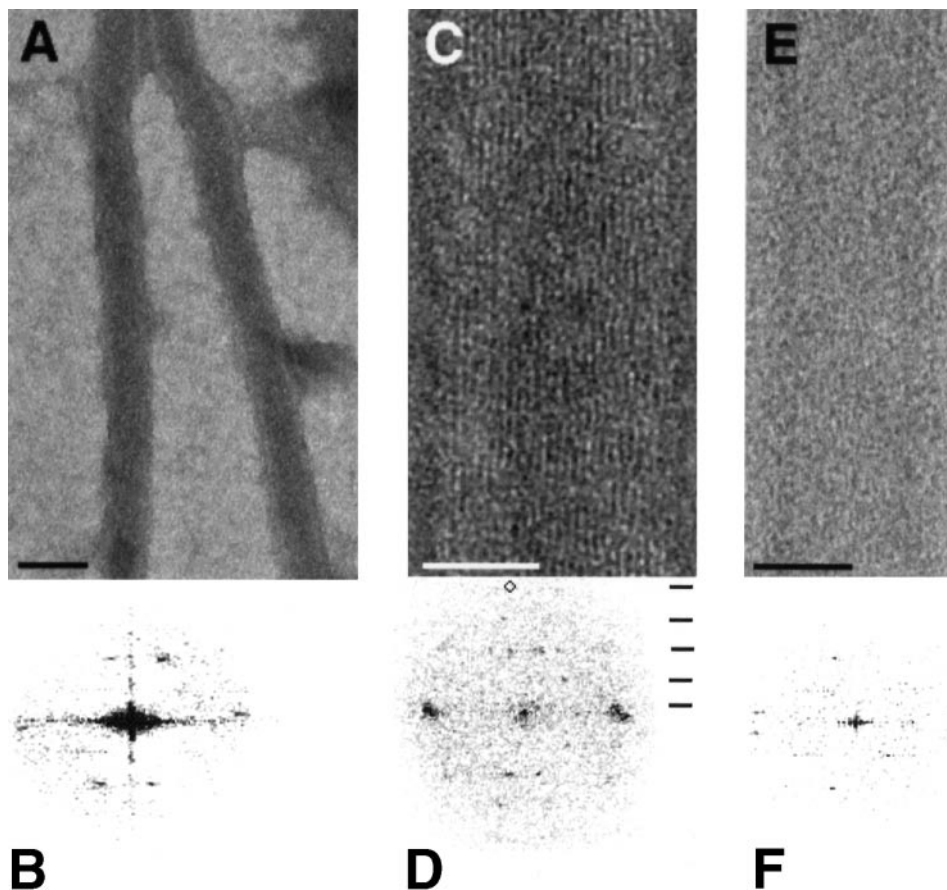


FIG. 2. IgG tubules formed from DNP-PE:PC monolayers. Under conditions similar to those that produce crystals (Uzgiris and Kornberg, 1983), micrometer-long helical tubules were observed. (A) Tubules grown on DNP-PE:PC monolayer in IgG Buffer B (pH 8.2). The typical tubule diameter varies from ~ 50 to 70 nm. (B) Summed Fourier transforms from several short, straight, well-ordered segments along the tubules. (C) A flattened tubule, characteristic of a type often observed, with two superimposed planar crystalline arrays. (D) The computed Fourier transforms of these arrays are much better ordered and frequently have reflections extending out to $1/2.9$ nm $^{-1}$ (circle, $IQ = 3$) or beyond. (E) Tubule preserved in vitreous ice. Tubules were prepared as in (A) and transferred to holey film-covered nickel grids. The sample was blotted and rapidly plunged into liquid ethane and stored in liquid nitrogen until use. The image was taken at $30,000\times$ magnification on a Jeol 1200EX microscope operating at an electron dose of ~ 6 e $^{-}/\text{\AA}^2$, as described previously (Avila-Sakar and Chiu, 1996). Tubule images that displayed strong optical diffraction were digitized and the Fourier transform was computed (F). In general, the transforms resemble those of the negatively stained samples, although there is some variability in the axial position of the first strong layer line. Layer lines in B correspond to the same resolutions as in Fig. 1, except the near-equatorial line, which is at $1/39.8$ nm $^{-1}$. Scale bars are (A) 100 nm, (C) 50 nm, (E) 50 nm. Lines in D correspond to the same resolutions as in Fig. 1.

TABLE I
IgG Tubule Conditions

	Ranges that allow PC-IgG tubule formation	No PC-IgG tubules formed	GalCer-IgG tubule conditions
% DNP-PE	5-20% DNP-PE	>20% DNP-PE	30% DNP-PE
Filler lipid	Egg-PC or DOPC	Plant-PC	GalCer
pH	8.2-8.5	<8.2	7.4
Grid types	Ni, Mo	Cu, Ti, Au, Au-plated Cu, stainless steel	Cu
Time	15-72 h	3 h	~ 15 h
[IgG]	0.2-0.3 mg/ml	<0.2 mg/ml	0.2 mg/ml
DTT	—	2 mM	—

due to the limited number of helical repeats present in the image and possibly from artifacts introduced by negative stain, some interesting conclusions can still be drawn. First, the end-on view clearly shows a central ring of density surrounded by seven individual densities, consistent with our expectation of a central lipid bilayer core to which individual proteins are bound in a helical arrangement. The diameter of the entire lipid cylinder is ~ 18 nm and the width of the bilayer is ~ 5 nm, similar to bilayer widths measured by low-angle X-ray scattering of phosphatidylcholine mixtures with varying acyl chains (Caffrey and Feigenson, 1981).

We have isolated the repeating density in the reconstruction (Fig. 4) and superimposed it on indi-

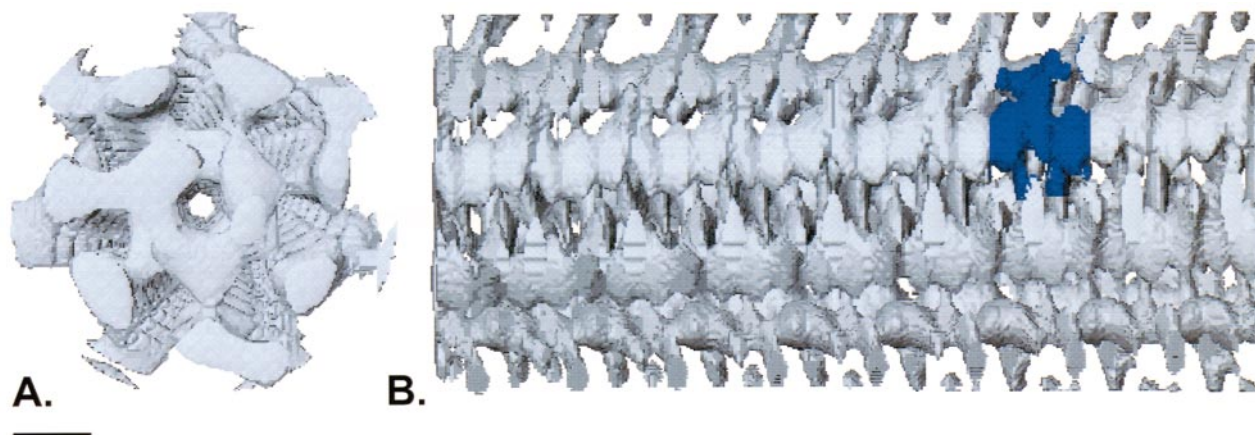


FIG. 3. Helical reconstruction of IgG κ 1 tubules grown on DNP-PE:DOPC lipids. The helical reconstruction was generated from a single negatively stained image that was representative of the majority of tubule images. (A) End-on view of the IgG-lipid tubule. The central continuous ring of density is likely the lipid tubule. (B) Side view of the reconstruction, showing the shallow helical pitch consistent with a 239-nm helical repeat. Highlighted in dark blue is the repeating unit, likely corresponding to a single IgG molecule. Scale bar, 100 Å.

vidual F_{ab} and F_c domains from the X-ray crystallographic structure of an IgG $_{2a}$ monoclonal (Harris *et al.*, 1997) displayed at 4-nm resolution. The placement is far from certain, but suggests that these fragments are consistent in shape and size with our reconstruction. Furthermore, both F_{abs} are best oriented with their combining regions facing the lipid surface, suggesting that each likely makes contact with the haptenated lipid.

G_t-Lipid Tubule Growth

G_t is a naturally membrane-bound protein and, unlike IgG, conditions for the two-dimensional or helical crystallization of G_t have not previously been published. Therefore we screened through a wide range of conditions using the lipid layer technique before we succeeded in forming G_t -lipid tubules. G_t is an anionic protein at neutral pH, and under

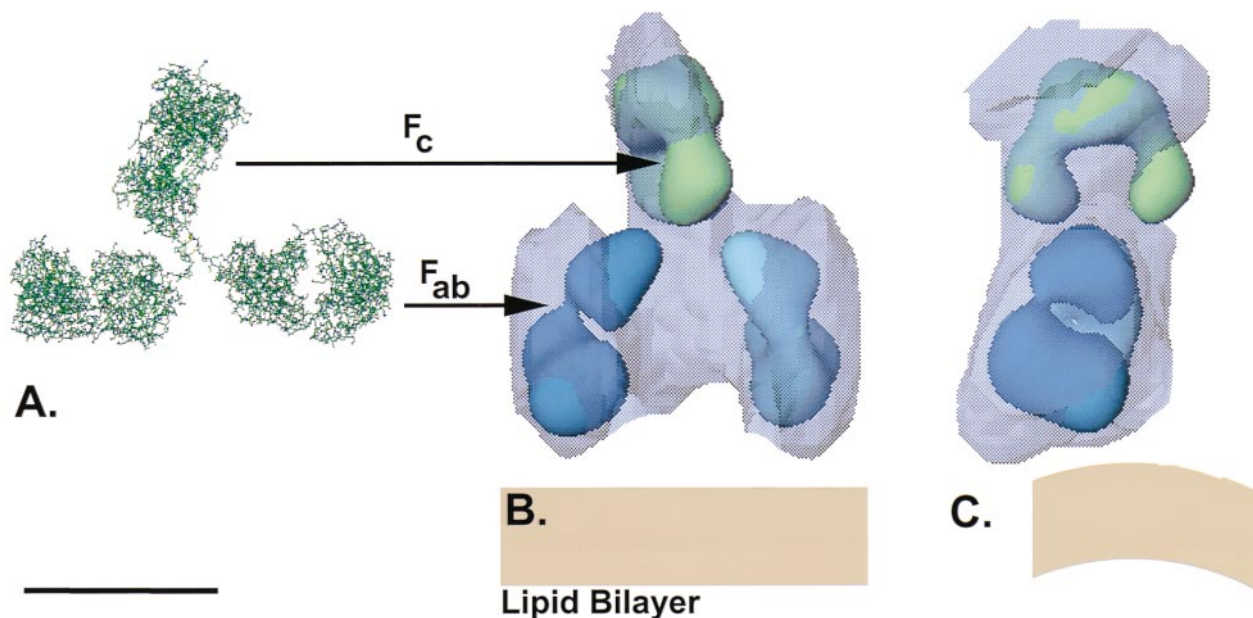


FIG. 4. Comparison of the repeating density with a known IgG structure. The X-ray structure of IgG $_{2a}$ molecule (A) was displayed at 4-nm resolution (highlighted domains in B and C), similar to the resolution of our helical reconstruction. The repeating density in the helical reconstruction (B and C) compares favorably with the overall size of the X-ray structure. The lower two domains in the figure are in close proximity to the lipid surface and are likely to be F_{abs} . Because the regions between the F_c and the F_{ab} domains of IgG are known to be flexible, we visually fit each domain into the reconstruction independently (B and C). Scale bar, 75 Å.

hypotonic conditions we detected increased binding (either by radioactive labeling or by electron microscopy) to positively charged monolayers that were transferred to EM grids. The tubules were grown on the cationic lipid mixture 20:80 mol/mol DOTAP:diphytanoyl-PC and formed in as little as 20 min but peaked in number around 2 h (Figs. 5B and 5C). With highly purified G_t , no tubular structures were seen in the absence of lipid. G_t tubules are about 27 nm in diameter and can grow to several micrometers in length. The tubules display a variety of helical symmetries as evidenced by the differences in computed Fourier transforms (Figs. 5D–5F); however,

the majority appear to fall into a single class exemplified by the transform in Fig. 5D. This class has strong layer lines at 8- and 4-nm resolution, which correspond to the strong regular spacing of the striations seen in the tubule image.

Tubule formation is restricted to highly specific protein and lipid conditions (Table II) and did not occur with lipids alone. Replacement of the unsaturated lipid DOTAP with the saturated but otherwise similar lipid DSTAP prevents tubule formation, despite the fact that the same replacement is tolerated in small planar arrays of G_t (T.J.M., unpublished observations). Incorporation of small quantities of

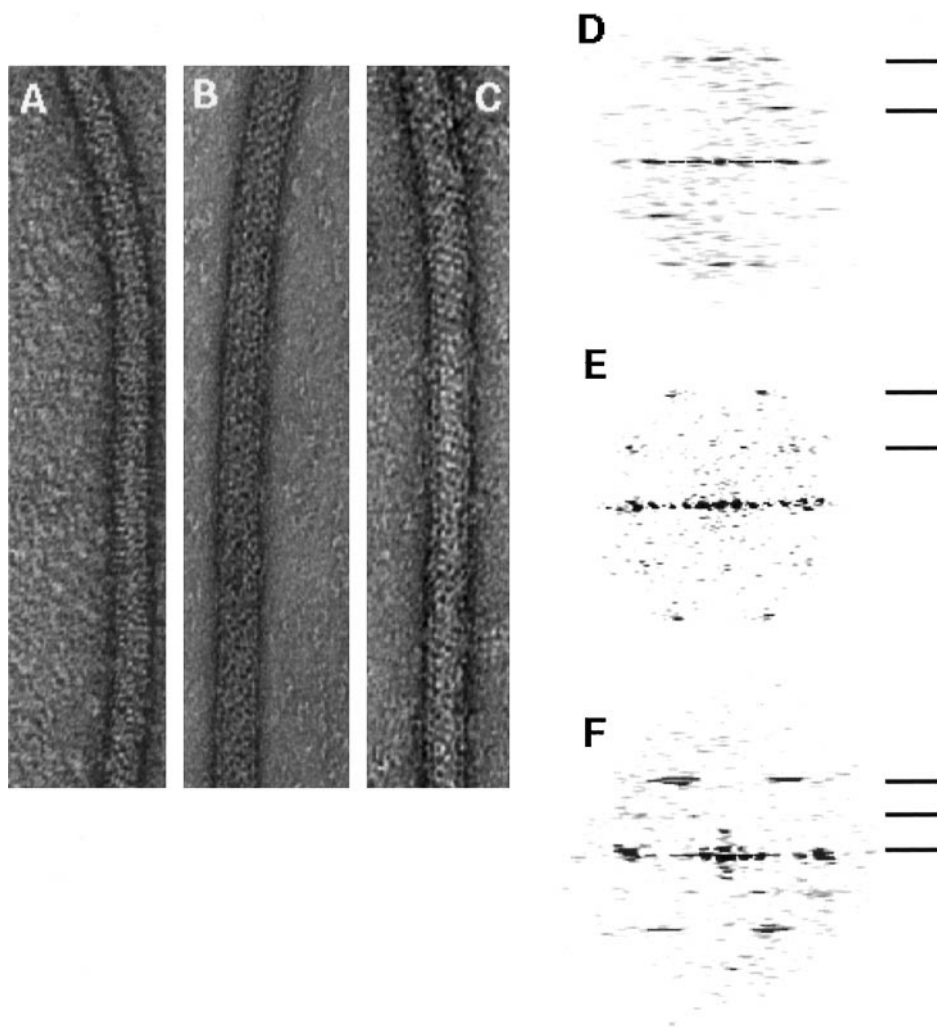


FIG. 5. G_t forms helical tubules on different lipid surfaces. (A) Crude G_t , which is >85% pure but still contains some residual retinal-derived lipids, forms helical tubules. After extraction, G_t was diluted into G_t tubule buffer to 0.2 mg/ml, allowed to incubate for 30–120 min, and applied to carbon-coated holey film grids. While tubules were observed belonging to a number of different helical families, the most common gave rise to computed transforms of the kind shown in (D). (B) Highly purified G_t did not form ordered arrays alone, but in the presence of a DOTAP:Diphytanoyl-PC monolayer, the long helical tubules shown were produced. (C) In the presence of Ca^{2+} more tubules were produced, with similar dimensions and order. Fourier transforms of these tubules reveal that they belong to many different helical families (e.g., E and F), but most resemble the dominant pattern shown in (D) for retinal-derived lipid tubules. All computed Fourier transforms are from straight segments of individual tubules. Lines in D and E correspond to $1/80$ and $1/40$ nm^{-1} . Lines in F correspond to $1/100$ and $1/50$ nm^{-1} .

TABLE II
G_t Tubule Conditions

	Conditions	Tubule numbers ^a
Standard conditions	20:80 DOTAP:diphytanoyl-PC + highly purified G _t in G _t tubule buffer	100%
Other lipid mixtures	20:80 DSTAP:diphytanoyl-PC	0%
	20:80 DOTAP:DOPC	0%
	1:20:79 FITC-PE:DOTAP:diphytanoyl-PC	~1%
	20:80 DOTAP:brominated-PC	<1%
	All other lipid mixtures tried	0%
Activation of G _t	Activation by GTPγS on ROS membranes	0%
	Activation by AIF3, either before or after tubule formation	0%
Ionic strength Cations	Addition of 100 mM NaCl	0%
	Increased Mg ²⁺ up to 10 mM	>100%
	Addition of Ca ²⁺ up to 10 mM	>100%
	Addition of EDTA or EGTA	0%
Crude G _t	Addition of TPEN	>100%
	Sempure crude G _t + endogenous lipids	<5%

^a Tubules counted per grid square by electron microscopy of several grids relative to standard conditions.

lipids with modified acyl chains or headgroups also dramatically reduced successful tubule formation.

Influence of Divalent Cations on Tubule Growth

G_t tubules formed only at relatively low ionic strength (<20 mM), but displayed a specific requirement for divalent cations. No tubules were formed without Mg²⁺, and Ca²⁺ enhanced tubule formation. The addition of the chelator TPEN, which binds transition metals but not Mg²⁺ or Ca²⁺, further enhanced tubule formation, suggesting that small quantities of contaminating heavy metals are inhibitory, possibly by competing for binding of Mg²⁺ or Ca²⁺. One possible role of divalent cations may be to bridge anionic G_t molecules and further stabilize protein-protein contacts.

G_t Tubules Can Form on Endogenous Lipids

While highly purified G_t requires a very specific lipid mixture in the monolayer in order to form tubules, crude G_t can form tubules completely independently of an exogenous lipid monolayer simply by dilution into G_t tubule buffer (Fig. 5A). In this case, less than 5% of the total G_t exists in helical arrays, as determined from tubule pelleting assays, consistent with the limited amount of lipid that is still present

in this crude protein. Phosphate analysis indicates that this protein contains about two residual phospholipids for every G_t. Given that the surface area of G_t interacting with the membrane should occlude 30–50 phospholipids (depending on orientation) and that the membrane is a bilayer, we would predict that each G_t in a tubule would require 60–100 phospholipids. With residual phospholipid totaling only 2/G_t, we would predict that tubule formation would be reduced to 1–3% of total G_t, consistent with our pelleting result. Interestingly, the stability of these arrays is sensitive to all of the same parameters in Table II as the arrays formed on cationic lipids, including the loss of tubules if the protein solution is introduced under an inappropriate lipid mixture. Sensitivity to the added lipids suggests that there is a competition between the small quantity of residual endogenous lipid present in the protein preparation and the vast excess of lipid provided by the monolayer for binding of G_t. The dimensions and helical order of these arrays are also similar to those formed on cationic lipids. As such, they provide evidence that the formation of tubule arrays, and therefore the orientation and binding of G_t on these lipids, is not limited to cationic surfaces, but instead mimics a binding and packing of G_t onto endogenous retinal-derived lipids, under some conditions.

Activation of G_t Destroys G_t-Lipid Tubules

Activation of G_t with aluminum fluoride stabilizes G_{tα} in a transition-like state and causes the separation of G_{tα} and G_{tβγ} subunits (Antonny and Chabre, 1992; Bigay *et al.*, 1985). Activation with aluminum fluoride, which occurs in the absence of receptor (Bigay *et al.*, 1985), also prevents tubule formation and is sufficient to eliminate tubules that have already formed (Fig. 6). In the latter case, the tubules are reduced to small vesicular structures or very small (<50 nm) cylindrical structures with no apparent helicity. Preactivation of G_t on ROS membranes with the nonhydrolyzable analog GTPγS also causes subunit separation and eliminates the ability to form tubules. Sensitivity to GTPγS and aluminum fluoride indicates that heterotrimeric G_t is necessary for tubule formation.

DISCUSSION

Comparisons of Tubule Forming Parameters

The results presented here, as well as previous studies of tubule formation, indicate that lipid composition is one of the most important parameters for formation of helical arrays. Theoretical descriptions of the formation of lipid tubules with large diameters (~500 nm) suggest that highly ordered interactions

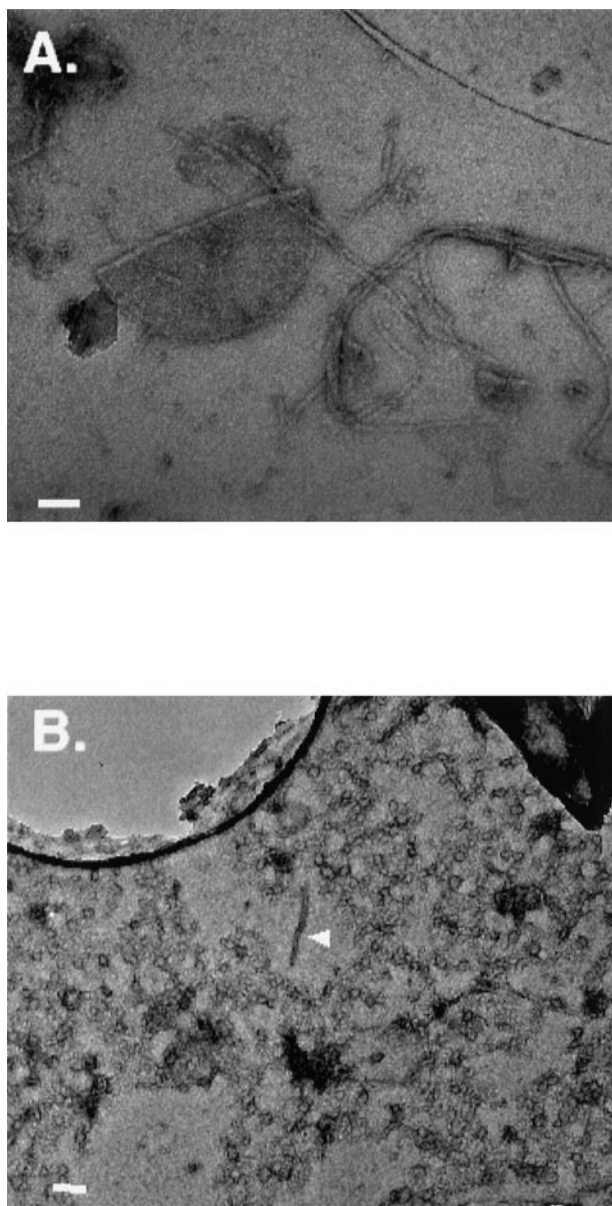


FIG. 6. Activation of G_t causes the lipid tubules to vesiculate. Activation with either the nonhydrolyzable analog GTP γ S or with the transition state stabilizer AlF_4^- results in a separation of the α and $\beta\gamma$ subunits and loss of tubule stability. (A) Field of G_t tubules grown on DOTAP-diphytanoyl-PC monolayers in G_t tubule buffer plus 1 mM NaCl. (B) G_t in G_t tubule buffer activated with 1 mM NaF and 30 μ M $AlCl_3$ before a DOTAP-diphytanoyl-PC monolayer was layered over the solution. While the majority of the structures are vesicular, some small disordered tubules remain (arrowhead). Similar vesiculation was observed if tubules were formed first and then G_t was activated. Scale bars are 100 nm in both panels.

between chiral lipid molecules induce a curvature in the lipid bilayer (Schnur, 1993). The degree of curvature is related both to the chiral nature of the lipid and to the degree of unsaturation that determines the ratio of the surface area occluded by the lipid

headgroup to the area occluded by the acyl chains. A dependence on these parameters was also observed for small-diameter tubules containing biotinylated lipids (Huetz *et al.*, 1997) that were used for the helical crystallization of streptavidin (Ringler *et al.*, 1997).

A comparison of the results with IgG and G_t suggests that for any given protein, various lipid mixtures can support tubule formation, but for each tubule-forming mixture, there is fairly low tolerance to changes in lipid composition. For example, G_t tubules do not form when the unsaturated DSTAP is substituted for DOTAP. However, endogenous lipids, of uncertain composition, but containing no cationic lipids whatsoever, also support formation of G_t tubules. Similarly, replacement of egg-PC, which contains predominantly palmitic acid, with plant-PC, which contains over 60% linoleic acid, eliminates IgG tubule formation, but tubules also formed when there was no PC present, and GalCer was used instead.

For G_t , unlike IgG, the lipids covalently attached to the protein are likely important for determining which lipid mixtures support ordered tubule formation. Disorder introduced into the hydrocarbon phase by the diphytanoyl methyl groups may facilitate insertion of the fatty acyl and isoprenoid tethers. A related phenomenon is the improved binding and activation of a complex of activated $G_{t\alpha}$ and cGMP phosphodiesterase (another doubly lipidated peripheral membrane protein) on unsaturated, compared to saturated, phosphatidylcholine vesicles (J. A. Malinski and T. G. Wensel, unpublished observations).

An interesting feature of both sets of tubules (IgG and G_t) is the very tight radius of curvature of the central lipid layer. The radius of the G_t -lipid tubule is only 13.5 nm, of which 5–9 nm can be attributed to protein, depending on orientation. Therefore the radius of curvature (R_c) for the central lipid tubule must be 4.5–8.5 nm, similar to or smaller than the smallest R_c s observed for phosphatidylcholine liposomes (7.5–10 nm: (Brouillette *et al.*, 1982; Mason and Huang, 1978)). To maintain this very small radius, the lipids in the inner leaflet of the vesicle bilayer must twist their headgroups out of plane and maintain a highly ordered alignment to avoid overlapping with adjacent lipids (Brouillette *et al.*, 1982). Assuming similar constraints are present in the G_t -lipid tubules, the low tolerance for lipids with other headgroup structures, and in particular for lipids conjugated with additional moieties such as FITC-PE (see Table II), is not surprising. For both proteins, computed FTs from the assemblies obtained with very different lipid mixtures suggested

similar if not identical packing of protein subunits, indicating that in each tubule the protein binds the membrane surface in a similar orientation. For IgG it seems obvious that the lipid-binding site must be at the interface between the F_{ab} and the DNP moiety, and therefore the protein orientation is probably restricted. G_t requires its lipid-modified termini (Fukada *et al.*, 1990; Yang and Wensel, 1992) in order to bind neutral lipid membranes (Yang, 1993), and X-ray crystallographic structures of G_t and the highly related G_i suggest that these modifications are probably very close to one another (Lambright *et al.*, 1996; Wall *et al.*, 1995), perhaps acting as a single-point tether to the membrane surface. Given that the entire surface of G_t is highly anionic, one might have expected its binding to anionic endogenous membranes and to the cationic tubules to involve very different faces of the protein. Therefore it is somewhat surprising that comparisons of the FTs indicate nearly identical lattices, consistent with a single, highly preferred, protein orientation.

Other studies have noted changes in antibody packing and crystalline lattice with pH changes (Reidler *et al.*, 1986; Uzgiris, 1990), suggesting that low and high pH values optimize different sets of protein-protein interactions. The two sets of IgG tubules formed on very different lipids as well as at different pH values yet appear to involve similar protein packing (based on similarities in the computed FTs). Thus lipid composition and pH may contribute quantitatively to the overall stability of the structure without drastically altering protein-protein interactions.

G_t Activation within the Helical Array

Because there is no evidence that G_t forms helical arrays in the cell, it was important to determine whether it retains its normal functional properties in the helical arrays. Perhaps the most important function of G_t is the conformational change and subunit dissociation it undergoes upon binding of GTP or an analogue (Fung, 1983). We were able to induce this activity *in situ* with the tubules by adding AlF_4^- , which has long been known to induce a GTP-like conformation of G_t , as evidenced by dissociation of the G_α and $G_{\beta\gamma}$ subunits and by the ability to activate the effector enzyme, cGMP phosphodiesterase (Bigay *et al.*, 1985; Stein *et al.*, 1985). Indeed, treating G_t tubules with this activating reagent leads to a dramatic structural change consistent with subunit dissociation. The small vesicular structures that result from G_t activation are reminiscent of those observed after activation of dynamin and subsequent vesiculation of its tubule arrays (Sweitzer

and Hinshaw, 1998; Takei *et al.*, 1998). The collapse of G_t tubules to vesicles is consistent with the observation that tubules are not readily formed by this lipid mixture in the absence of heterotrimeric G_t . Presumably the small R_c of the central lipid tubule is energetically unstable and therefore it is not surprising that the formation of this structure is dependent on protein-protein interactions and that changes in these interactions cause the tubular structures to collapse. Whether dynamin-mediated GTP hydrolysis initiates vesicle formation from tubules through a similar mechanism by simply disordering the dynamin helix, or instead represents a specific and distinct "pinching" mechanism for vesiculation, remains to be determined. However, it is intriguing that another GTPase, G_i , with no known role in membrane dynamics, shows similar behavior.

Helical Reconstruction of IgG

Although several groups have now developed conditions for the helical crystallization of soluble proteins on lipid tubules (Polyakov *et al.*, 1995; Ringle *et al.*, 1997; Sweitzer and Hinshaw, 1998; Takei *et al.*, 1998; Wilson-Kubalek *et al.*, 1998), only one has been used to generate a three-dimensional reconstruction (Darst *et al.*, 1998). Frequently the limiting step in generating such reconstructions is determining the correct indexing scheme for the layer lines in the Fourier transforms of the images. We were able to generate a preliminary reconstruction of the IgG tubules rapidly, because the indexing was fairly straightforward. All of the DNP-PE/DOPC tubules appear to belong to the same helical family and the presence of some well-ordered flattened tubules allowed the lattice to be determined as for planar arrays and then applied to indexing the layer lines for less flattened tubules.

Although we have made tentative assignments of protein domains to the different densities in the IgG reconstructions, these are by no means definitive, due to the limited number of helical repeats included in the processing and the relatively low resolution. However, it seems likely that contacts with the inner lipid tubule must be with individual F_{ab} domains; therefore the tilted and elongated domain furthest from the lipid surface represents the F_c region. As shown in Fig. 4, the X-ray crystallographic structure of each of these domains fits well in the predicted densities. This assignment is also consistent with the interpretations of projection structures from other IgG two-dimensional crystalline assemblies (Reidler *et al.*, 1986; Uzgiris and Kornberg, 1983). The rapidity with which such reconstructions can be generated, once the correct indexing scheme is determined, is one of the advantages of tubular crystals,

which should be particularly useful for determining structures of membrane complexes of peripheral membrane proteins, such as G_t .

The authors gratefully acknowledge the use of the facilities of the National Center for Macromolecular Imaging (RR02250), the helpful suggestions of Drs. Amy McGough and Justine A. Malinski, and support by the National Eye Institute (EY07981, EY07001), NASA (NAG8 1387), the Welch Foundation (Q-1179), the National Library of Medicine (LM07093), and the Keck Center for Computational Biology.

REFERENCES

- Antonny, B., and Chabre, M. (1992) Characterization of the aluminum and beryllium fluoride species which activate transducin, *J. Biol. Chem.* **267**, 6710–6718.
- Avila-Sakar, A. J., and Chiu, W. (1996) Visualization of beta sheets and side-chain clusters in 2-dimensional periodic arrays of streptavidin on phospholipid monolayers by electron crystallography, *Biophys. J.* **70**, 57–68.
- Bigay, J., Deterre, P., Pfister, C., and Chabre, M. (1985) Fluoroaluminates activate transducin-GDP by mimicking the gamma-phosphate of GTP in its binding site, *FEBS Lett.* **191**, 181–185.
- Brouillette, C. G., Segrest, J. P., Ng, T. C., and Jones, J. L. (1982) Minimal size phosphatidylcholine vesicles: Effects of radius of curvature on head group packing and conformation, *Biochemistry* **21**, 4569–4575.
- Caffrey, M., and Feigenson, G. W. (1981) Fluorescence quenching in model membranes. 3. Relationship between calcium adenosinetriphosphatase enzyme activity and the affinity of the protein for phosphatidylcholines with different acyl chain characteristics, *Biochemistry* **20**, 1949–1961.
- Chen, P. S., Toribara, T. Y., and Warner, H. (1956) Microdetermination of phosphorous, *Anal. Chem.* **28**, 1756–1758.
- Darst, S. A., Polyakov, A., Richter, C., and Zhang, G. (1998) Insights into *Escherichia coli* RNA polymerase structure from a combination of X-ray and electron crystallography, *J. Struct. Biol.* **124**, 115–122.
- DeRosier, D. J., and Moore, P. B. (1970) Reconstruction of three-dimensional images from electron micrographs of structures with helical symmetry, *J. Mol. Biol.* **52**, 355–369.
- Fukada, Y., Takao, T., Ohguro, H., Yoshizawa, T., Akino, T., and Shimonishi, Y. (1990) Farnesylated gamma-subunit of photoreceptor G protein indispensable for GTP-binding, *Nature* **346**, 658–660.
- Fukami, A., and Adachi, K. (1965) A new method of preparation of a self-perforated micro plastic grid and its application, *J. Electron Microsc.* **14**, 112–118.
- Fung, B. K. (1983) Characterization of transducin from bovine retinal rod outer segments. I. Separation and reconstitution of the subunits, *J. Biol. Chem.* **258**, 10495–10502.
- Fung, B. K.-K., Hurley, J. B., and Stryer, L. (1981) Flow of information in the light-triggered nucleotide cascade of vision, *Proc. Natl. Acad. Sci. USA* **78**, 152–156.
- Hardt, S., Wang, B., and Schmid, M. F. (1996) A brief description of I.C.E.: The integrated crystallographic environment, *J. Struct. Biol.* **116**, 68–70.
- Harris, L. J., Larson, S. B., Hasel, K. W., and McPherson, A. (1997) Refined structure of an intact IgG2a monoclonal antibody, *Biochemistry* **36**, 1581–1597.
- Hinshaw, J., and Schmid, S. (1995) Dynammin self-assembles into rings suggesting a mechanism for coated vesicle budding, *Nature* **374**, 190–192.
- Huetz, P., Van Neuren, S., Ringler, P., Kermer, F., Van Breemen, J. F. L., Wagenaar, A., Engberts, J. B. F. N., Fraaije, J. G. E. M., and Brisson, A. (1997) Relationship between molecular structure and supramolecular morphology of DODA-EO₂-biotin and related lipids, *Chem. Phys. Lipids* **89**, 15–30.
- Lambright, D. G., Sondek, J., Bohm, A., Skiba, N. P., Hamm, H. E., and Sigler, P. B. (1996) The 2.0 Å crystal structure of a heterotrimeric G protein, *Nature* **379**, 311–319.
- Mason, J. T., and Huang, C. (1978) Hydrodynamic analysis of egg phosphatidylcholine vesicles, *Ann. N.Y. Acad. Sci.* **308**, 29–49.
- Melia, T. J., Cowan, C. W., Angleson, J. K., and Wensel, T. G. (1997) A comparison of the efficiency of G protein activation by ligand-free and light-activated forms of rhodopsin, *Biophys. J.* **73**, 3182–3191.
- Navon, S. E., and Fung, B. K. (1984) Characterization of transducin from bovine retinal rod outer segments: Mechanism and effects of cholera toxin-catalyzed ADP-ribosylation, *J. Biol. Chem.* **259**, 6686–6693.
- Polyakov, A., Severinova, E., and Darst, S. A. (1995) Three-dimensional structure of *E. coli* core RNA polymerase: Promoter binding and elongation conformations of the enzyme, *Cell* **83**, 365–373.
- Reidler, J., Uzgiris, E. E., and Kornberg, R. D. (1986) Two dimensional crystals of immunoglobulins, *Handb. Exp. Immunol.* **1**, 17.1–17.5.
- Ringler, P., Muller, W., Ringsdorf, H., and Brisson, A. (1997) Functionalized lipid tubules as tools for helical crystallization of proteins, *Chem. Eur. J.* **3**, 620–625.
- Schmid, M. F., Dargahi, R., and Tam, M. W. (1993a) SPECTRA: A system for processing electron images of crystals, *Ultramicroscopy* **48**, 251–164.
- Schmid, M. F., Robinson, J. P., and DasGupta, B. R. (1993b) Direct visualization of botulinum neurotoxin-induced channels in phospholipid vesicles, *Nature* **364**, 827–830.
- Schnur, J. M. (1993) Lipid tubules: A paradigm for molecularly engineered structures, *Science* **262**, 1669–1676.
- Stein, P. J., Halliday, K. R., and Rasenick, M. M. (1985) Photoreceptor GTP binding protein mediates fluoride activation of phosphodiesterase, *J. Biol. Chem.* **260**, 9081–9084.
- Sweitzer, S. M., and Hinshaw, J. E. (1998) Dynammin undergoes a GTP-dependent conformational change causing vesiculation, *Cell* **93**, 1021–1029.
- Takei, K., Haucke, B., Slepnev, V., Farsad, K., Salazar, M., Chen, H., and De Camilli, P. (1998) Generation of coated intermediates of clathrin-mediated endocytosis on protein-free liposomes, *Cell* **94**, 131–141.
- Takei, K., McPherson, P. S., Schmid, S. L., and De Camilli, P. (1995) Tubular membrane invaginations coated by dynammin rings are induced by GTP-gamma S in nerve terminals, *Nature* **374**, 186–190.
- Toyoshima, C. (1989) On the use of holey grids in electron crystallography, *Ultramicroscopy* **30**, 439–444.
- Uzgiris, E. E. (1990) Antibody organization on lipid films: Influence of pH and interchain disulfide reduction, *Biochem. J.* **272**, 45–49.
- Uzgiris, E. E., and Kornberg, R. D. (1983) Two-dimensional crystallization technique for imaging macromolecules, with an application to antigen-antibody-complement complexes, *Nature* **301**, 125–129.
- Wall, M. A., Coleman, D. E., Lee, E., Iniguez-Lluhl, J. A., Posner, B. A., Gilman, A. G., and Sprang, S. R. (1995) The structure of the G protein heterotrimer $G_{i\alpha}\beta_{1\gamma 2}$, *Cell* **83**, 1047–1058.

- Wensel, T. G. (1999) Heterotrimeric G proteins: Structure, regulation, and signaling mechanisms, in Sitaramayya, A. (ed.), *Introductory Signal Transduction*, pp. 29–46, Birkhauser, Boston.
- Wilson-Kubalek, E. M., Brown, R. E., Celia, H., and Milligan, R. A. (1998) Lipid nanotubes as substrates for helical crystallization of macromolecules, *Proc. Natl. Acad. Sci. USA* **95**, 8040–8045.
- Yang, Z. (1993) Studies of retinal inorganic pyrophosphatase and N-myristoylation of transducin, Verna and Marrs McLean Biochemistry Department, Baylor College of Medicine, Houston.
- Yang, Z., and Wensel, T. G. (1992) N-myristoylation of the rod outer segment G protein, transducin, in cultured retinas, *J. Biol. Chem.* **267**, 23197–23201.